Abnormal Elasticity of Single-Crystal Magnesiosiderite across the Spin Transition in Earth's Lower Mantle

Suyu Fu, Jing Yang, and Jung-Fu Lin

Phys. Rev. Lett. **118**, 036402 — Published 19 January 2017

DOI: 10.1103/PhysRevLett.118.036402

Abnormal elasticity of single-crystal magnesiosiderite across the spin transition in Earth's lower mantle

Suyu Fu[1], Jing Yang[1], Jung-Fu Lin[1*]

[1]*Department of Geological Sciences, Jackson School of Geosciences, The University of Texas at Austin, Austin, TX78712, USA*

**Corresponding author: Jung-Fu Lin (afu@jsg.utexas.edu)*

Abstract

Brillouin Light Scattering and Impulsive Stimulated Light Scattering have been used to determine the full elastic constants of magensiosiderite [$(Mg_{0.35}Fe_{0.65})CO_3$] up to 70 GPa at room temperature in a diamond anvil cell. Drastic softening in C_{11}, C_{33}, C_{12}, and C_{13} elastic moduli associated with compressive stress component and stiffening in C_{44} and C_{14} moduli associated with the shear stress component are observed to occur within the spin transition between ~42.4 and ~46.5 GPa. Negative values of C_{12} and C_{13} are also observed within the spin transition region. The Born criteria constants for the crystal remain positive within the spin transition, indicating that the mixed-spin state remains mechanically stable. Significant auxeticity can be related to the electronic spin transition-induced elastic anomalies based on the analysis of Poisson's ratio. These elastic anomalies are explained using a thermoelastic model for the rhombohedral system. Finally, we conclude that mixed-spin state ferromagnesite, which is potentially a major deep-carbon carrier, is expected to exhibit abnormal elasticity, including a negative Poisson's ratio of -0.6 and drastically reduced V_P by 10%, in the Earth's mid lower mantle.

Introduction

Elastic anomalies have been reported to occur across structural, electronic, and magnetic transitions at variable pressure and/or temperature (P-T) conditions in materials of interest to materials science, geoscience, and condensed matter physics including (Ca,Sr)TiO_3 perovskite [1-3], SiO_2 stishovite [4, 5], (Mg,Fe)O ferropericlase [6-9], Fe_3O_4 magnetite [10], FeO [11-13] and Fe-C systems [14, 15]. As the fourth-rank tensor linking a crystal's elastic strain response to external stress, elastic moduli, C_{ij}, can be very sensitive to changes in structural, electronic, magnetic, and phononic states. Therefore, examining crystals' elasticity under changing thermodynamic conditions is an effective means to elucidate the interplay of the aforementioned physical states of a given crystal [16]. Due to technical and theoretical limitations, however, few studies have combined both experimental and theoretical techniques to describe crystal elasticity across a transition.

Landau theory can be used to attribute the structural-induced elastic anomalies to a spontaneous strain in crystals [17, 18]. This method, which involves analysis of the Landau expansion for specific crystal structures, is generally in agreement with experimental results [1-4]. Elastic anomalies have also been reported to occur within magnetic and electronic transitions of iron at extreme P-T conditions that are of great interest to materials science as well as deep-Earth research, as iron is the most abundant transition metal in the planet's interior [19]. For example, phonon-magnon coupling in Fe_3C [15] and FeO [11-13] has been used to explain the observed anomalous shear softening across their respective magnetic transitions. Additionally, an electronic spin transition of iron from high-spin (HS) to low-spin (LS) states has been recently reported to occur in several Fe-bearing systems, including ferropericalse [8, 20], bridgmanite [21], ferromagnesite [22, 23], and FeOOH [24]. A thermoelastic model for cubic crystals has been developed to explain the observed elastic anomalies across the spin transition in ferropericlase [9]. The development of the thermoelastic theory and simultaneous experimental measurements of the elasticity for cubic ferropericlase have greatly advanced our understanding of the condensed matter physics and geophysics of Fe-bearing materials across the spin transition at high pressures [8, 9, 25]. However, our understanding of the elastic anomalies across the electronic spin transition has been limited to the cubic crystal system, as consistent theoretical models and experimental results are not available for other crystal systems.

Potential effects of the spin transition on the elasticity and thermodynamics can occur in other crystal systems of lower symmetries, including the rhombohedrally-structured Fe-bearing magnesite, a potential deep mantle carbon carrier due to its abundance within subducted slabs and wide P-T stability [26-30]. Magnesite [$MgCO_3$] and siderite [$FeCO_3$] can form a solid solution series, which is generally called ferromagnesite for the $MgCO_3$-rich parts and magnesiosiderite for the $FeCO_3$-rich parts of the system [22, 23]. Fe^{2+} ions reside in the octahedral site of the ferromagnesite lattice, which is similar to ferropericlase, but the octahedra are strongly linked via triangular CO_3^{2-} units [22]. A sharp spin transition of iron in ferromagnesite has been reported to occur at approximately 45 GPa using several experimental and theoretical techniques including high pressure Mössbauer spectroscopy [31], X-ray emission spectroscopy [32], X-ray diffraction [23, 33], Raman spectroscopy [22], and first-principles calculations [34, 35]. Depending on the iron content, the spin transition is associated with an abrupt ~6-10% reduction in the unit-cell volume [23]. Furthermore, the occurrence of the dense low-spin ferromagnesite induces a structural transition to ferromagnesite II at higher pressures [36]. The sharp spin transition with a width of only ~4 GPa and a corresponding large volume reduction in ferromagnesite represents a case study for deciphering elastic anomalies across an electronic spin transition in lower-symmetry systems. Knowing the influence of the spin transition on the elasticity of ferromagnesite can improve our understanding of the physical and chemical behavior of this potential deep-carbon carrier in the lower mantle [27, 37].

In this Letter, we have measured the compressional wave (V_P) and shear wave (V_S) velocities of single-crystal magnesiosiderite [$(Mg_{0.35}Fe_{0.65})CO_3$] across the spin transition up to 70 GPa using Brillouin Light Scattering (BLS) and Impulsive Stimulated Light Scattering (ISS) in a diamond-anvil cell (DAC). Our derived full elastic constants of the crystal show that C_{11}, C_{33}, C_{12} and C_{13} elastic moduli associated with the compressive stress component drop drastically within the spin transition at ~45 GPa, while C_{44} and C_{14} elastic moduli associated with the shear stress component jump by 25% and 80%, respectively. These elastic behaviors are explained using a thermoelastic model for the rhombohedral crystal system that was developed in this study. The observed elastic anomalies are broadly discussed within the framework of the interplay between acoustic phonons and structural, electronic and magnetic transitions in materials of interests to geoscience, materials science, and condensed matter physics.

Results and Discussion

The combination of BLS and ISS techniques with a DAC enables us to measure both V_S and V_P of single-crystal magnesiosiderite [$(Mg_{0.35}Fe_{0.65})CO_3$] on the (101) cleavage platelet at pressures up to 70 GPa (Fig. 1). The measured V_P and V_S vary significantly as a function of the azimuthal angle, indicating strong elastic anisotropies of the sample at high pressures (Figs. 2 and S5). Based on the relationship of V_P and V_S as a function of the crystallographic direction, we have solved for the complete set of elastic constants of the rhombohedral magnesiosiderite using Christoffel's equations [38]. The density information of the crystal was taken from its equation of state reported in a previous X-ray diffraction study [23]. Using the derived C_{ij} of the crystal, the adiabatic bulk and shear moduli (K_S and G) were calculated using the Voigt-Reuss-Hill averages [39]. The calculated K_S and G at ambient conditions are K_{S0} = 180.0(9) and G_0 = 53.4(5) GPa, consistent with previous results within experimental uncertainties (Table S2).

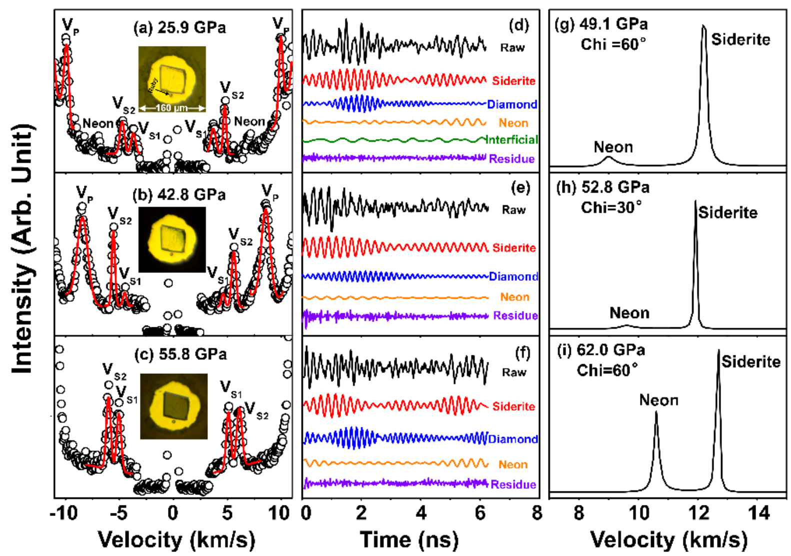

FIG. 1 (color online). Velocity measurements of the single-crystal magnesiosiderite [$(Mg_{0.35}Fe_{0.65})CO_3$] at high pressures and room temperature. In the Brillouin spectra (a,b,c), black open circles are experimental data and red lines are the best fit to the spectra. The inserted images show crystal color in the transmitted light at corresponding pressures. Using Fourier transformation, the time-dependent impulsive spectra (d,e,f) were modeled to derive the power spectra (g,h,i) in the frequency domain and the V_P of the sample at certain orientations (shown as Chi angle) at high pressures. Neon pressure medium was also detected in the BLS and ISS spectra at high pressures.

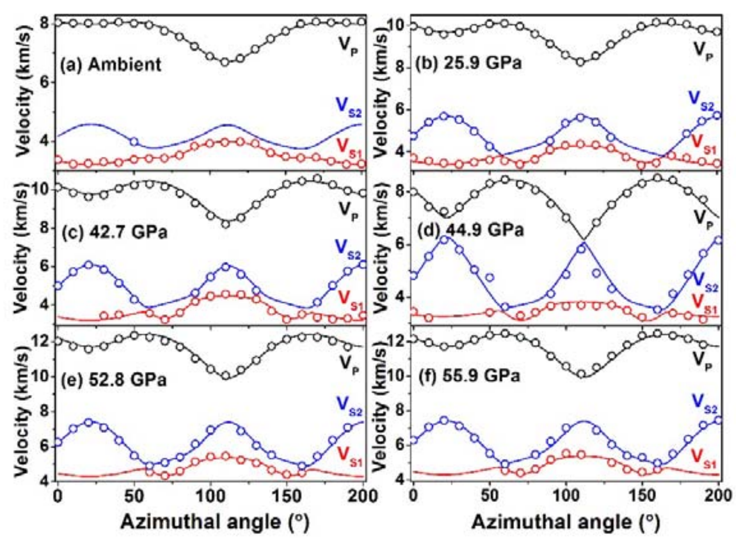

FIG. 2 (color online). Compressional (V_P) and shear (V_S) wave velocities of the single-crystal magnesiosiderite [$(Mg_{0.35}Fe_{0.65})CO_3$] as a function of the azimuthal angle at high pressures and room temperature. (a) and (b) show the high-spin (HS) states; (c) and (d) show the mixed-spin (MS) states; (e) and (f) show the low-spin (LS) states. Open circles represent experimental results, while solid lines represent the best fits to the experimental data using the Christoffel's equation.

Analysis of the six elastic constants of the single-crystal magnesiosiderite as a function of pressure show that they increase monotonically with increasing pressure below 42.4 GPa and above 46.5 GPa, which correspond to the onset and ending pressure of the spin transition, respectively (Fig. 3). Third-order Eulerian finite strain equations were used to obtain the first-order pressure derivatives of the elastic moduli for HS and LS states, yielding: $(\partial C_{11}/\partial P)_{300K} = 6.12(7)$, $(\partial C_{33}/\partial P)_{300K} = 2.76(2)$, $(\partial C_{44}/\partial P)_{300K} = 1.70(1)$, $(\partial C_{12}/\partial P)_{300K} = 4.38(3)$, $(\partial C_{13}/\partial P)_{300K} = 3.72(3)$, and $(\partial C_{14}/\partial P)_{300K} = 1.08(1)$ for the HS state, and $(\partial C_{11}/\partial P)_{300K} = 3.2(2)$, $(\partial C_{33}/\partial P)_{300K} = 8.7(5)$, $(\partial C_{44}/\partial P)_{300K} = 2.3(2)$, $(\partial C_{12}/\partial P)_{300K} = 3.3(3)$, $(\partial C_{13}/\partial P)_{300K} = 8.9(4)$, and $(\partial C_{14}/\partial P)_{300K} = 0.9(2)$ for the LS state (Table S3). Comparing the elastic constants of the pure HS state with that of pure LS state, their values in the LS state are, in all cases except for C_{12}, higher than that of the extrapolated HS state. Based on the definition of the elastic constants: $C_{ij} = \frac{1}{V}\frac{\partial^2 E}{\partial\varepsilon_i \partial\varepsilon_j}|_0$, such differences between the HS and LS states can be attributed to the stiffer lattice of the LS state due to the collapse of the lattice across the spin transition. However, the pressure derivatives of the elastic constants behave quite differently: the LS state exhibits higher pressure derivatives of C_{33}, C_{44} and C_{13} than that of the HS state, but the pressure derivatives of C_{11}, C_{12} and C_{14} display the opposite behavior.

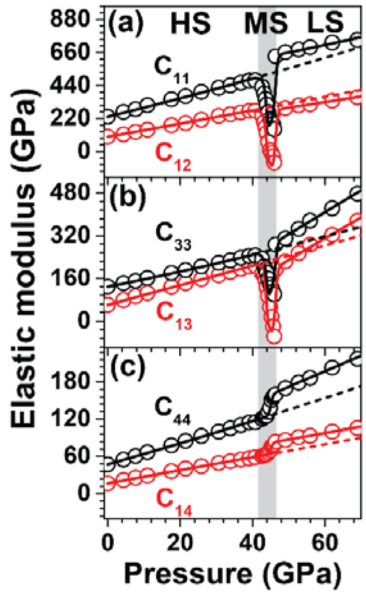

FIG. 3 (color online). Single-crystal elastic constants of magnesiosiderite [$(Mg_{0.35}Fe_{0.65})CO_3$] at high pressures and room temperature. Open circles: experimental results; solid lines: modeled results using the finite-strain fitting for the HS and LS states, respectively. Modelling for the MS state shown by the grey vertical line is based on the elasticity and thermodynamics theory. Dashed lines represent the extrapolated constants of the HS state.

Of particular interest are the observed elastic anomalies between 42.4 to 46.5 GPa: drastic softening occurs in four elastic constants, C_{11}, C_{33}, C_{12}, and C_{13}, while stiffening occurs in C_{44} and C_{14} (Fig. 3). This abnormal elastic behavior coincides with significant changes in Raman shifts and optical colors induced by the spin transition (Figs. S2 and S3) [22, 23, 33, 40]. Interestingly, C_{12} and C_{13} become negative at approximately 45.2 GPa, which is about midway through the spin transition. This indicates a significant shear elastic instability of the crystal. Based on the Born stability criteria [41], one can examine the mechanical stability of the rhombohedral crystal:

$$B_1 = C_{11} - |C_{12}| > 0 \tag{1}$$

$$B_2 = (C_{11} + C_{12})C_{33} - 2C_{13}^2 > 0 \tag{2}$$

$$B_3 = (C_{11} - C_{12})C_{44} - 2C_{14}^2 > 0 \tag{3}$$

Analysis of the Born criteria using these equations shows that $B_1 > 70\ GPa$, $B_2 > 600\ GPa^2$ and $B_3 > 5000\ GPa^2$. All the Born criteria constants remain positive throughout the spin transition, indicating that the crystal in the mixed-spin (MS) state, with negative C_{12} and C_{13}, remains mechanically stable. The shear elastic instability of the crystal, manifested in the negative C_{12} and C_{13}, is shown to be insufficient to mechanically destabilize the crystal within the spin transition.

To understand the effects of the spin transition on the elasticity of the crystal, we have used Eulerian finite-strain theory [42] to develop a general thermoelastic formulation for modelling the C_{ij} of the rhombohedral system at high pressures [9] (See Supplemental Material [43] for details). According to the extension of the thermoelastic model for the cubic ferropericlase [9], the elastic compliances S^{ij} of the rhombohedral crystal across the spin transition can be described as:

$$S^{ij}V(n) = nS_{LS}^{ij}V_{LS} + (1-n)S_{HS}^{ij}V_{HS} - \left(\frac{\partial G_{LS}}{\partial \sigma_j} - \frac{\partial G_{HS}}{\partial \sigma_j}\right)\frac{\partial n}{\partial \sigma_i} \quad (4)$$

where V is the unit-cell volume, n is the LS fraction, σ_i and σ_j are the *ith* and *jth* stress component, respectively, in the Voigt notation, and G is the Gibbs free energy. The expansion of the general formulation to the six elastic compliances of the rhombohedral crystal can be expressed as:

$$S^{11}V(n) = nS_{LS}^{11}V_{LS} + (1-n)S_{HS}^{11}V_{HS} - \frac{1}{9}(V_{LS} - V_{HS})\frac{\partial n}{\partial P} \quad (5)$$

$$S^{33}V(n) = nS_{LS}^{33}V_{LS} + (1-n)S_{HS}^{33}V_{HS} - \frac{1}{9}(V_{LS} - V_{HS})\frac{\partial n}{\partial P} \quad (6)$$

$$S^{44}V(n) = nS_{LS}^{44}V_{LS} + (1-n)S_{HS}^{44}V_{HS} \quad (7)$$

$$S^{12}V(n) = nS_{LS}^{12}V_{LS} + (1-n)S_{HS}^{12}V_{HS} - \frac{1}{9}(V_{LS} - V_{HS})\frac{\partial n}{\partial P} \quad (8)$$

$$S^{13}V(n) = nS_{LS}^{13}V_{LS} + (1-n)S_{HS}^{13}V_{HS} - \frac{1}{9}(V_{LS} - V_{HS})\frac{\partial n}{\partial P} \quad (9)$$

$$S^{14}V(n) = nS_{LS}^{14}V_{LS} + (1-n)S_{HS}^{14}V_{HS} \quad (10)$$

These equations were applied to model the high-pressure experimental C_{ij} data shown in Fig. 3. In the model, the low-spin fraction (n) and the unit-cell volume (V) were initially derived from the equation of state of the crystal reported previously [23] (See Supplemental Material [43] for details).

Examination of these equations and modelled results shows that the third term on the right-hand side of the Eq. (1) only appears in the mixed-spin state when $\partial n/\partial\sigma_i \neq 0$, where $i = 1, 2, 3$. That is, for C_{11}, C_{33}, C_{12}, and C_{13} elastic constants, which are related to the compressional stress component, an additional Gibbs free energy term associated with the mixed-spin state exists. Because a volume collapse is associated with the spin transition where $V_{LS} < V_{HS}$ and the $\partial n/\partial\sigma_i$ term is always positive, it follows that S^{11}, S^{33}, S^{12}, and S^{13} of the LS state must become larger than that in the pure HS state. Consequently, the drastic softening in C_{11}, C_{33}, C_{12}, and C_{13} elastic constants and in K_S and V_P occurs within the spin transition. However, the additional Gibbs free energy term is cancelled out because n is an even function of the shear stress components, in the Eqns. (4) and (7) for C_{44} and C_{14} elastic constants. Thus, C_{44} and C_{14} as well as G and V_S increase across the spin transition due to an increase in density associated with the collapsed unit cell.

Our modelled results and experimental values are remarkably consistent for the elasticity of the single-crystal magnesiosiderite across the spin transition at high pressures (Figs. 3 and 4). The C_{11} and C_{33} elastic constants are significantly softened by a maximum of 66% and 59% respectively, and C_{12} and C_{13} are softened so drastically that they become negative at around 45.2 GPa. On the other hand, C_{44} and C_{14} jump by 25% and 80%, respectively, across the spin transition. As a result, K_S decreases to almost zero within the spin transition, V_P drops by a maximum of 40%, and V_S and G are slightly enhanced. Furthermore, the LS state of magnesiosiderite has drastically different V_P and V_S anisotropies than that of the HS state. Within the spin transition, V_P anisotropy experience a sharp drop while V_S splitting anisotropy is enhanced and then drops. It should be noted that slight deviations between the experimental data and modelled curves may be due to a pressure gradient in sample chamber that can result in local inhomogeneity in the ratio of HS and LS states (Fig. S4).

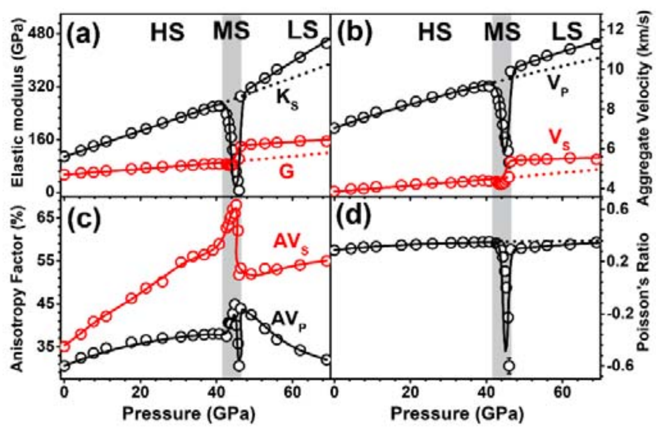

FIG. 4 (color online). Elastic parameters of magnesiosiderite [$(Mg_{0.35}Fe_{0.65})CO_3$] at high pressures. (a): adiabatic bulk (K_S) and shear modulus (G); (b): aggregate compressional (V_P) and shear (V_S) wave velocities; (c): V_P and V_S seismic anisotropy factors (AV_P, AV_S); (d): Poisson's ratio. Open circles: experimental results; solid lines: best modelled fits to experimental data. Solid lines in (c) are plotted to guide the eyes. Grey areas represent the mixed-spin state region.

Poisson's ratio is another important parameter to constrain the mechanical and acoustic wave properties of the crystal, and is often defined as: $\nu = \frac{1}{2}\left[\left(\frac{V_P}{V_S}\right)^2 - 2\right] / \left[\left(\frac{V_P}{V_S}\right)^2 - 1\right]$, in geoscience application [54]. Significant auxeticity (negative Poisson's ratio) across structural transitions has been reported to occur for the α-β structural transition in quartz [55] and the β-γ structural transition in isotropic In-Sn alloys [56]. Per the Landau theory for phase transformations, negative elastic moduli will occur as a phase boundary is approached via a change of thermodynamic variables. The elastic anomalies entail significant structural instability, followed by a structural transition [18]. Across the structural transition, the compressibility of the crystal increases abruptly, resulting in a drastic softening of the K/G ratio as well as Poisson's ratio, which could become negative. This auxetic behavior has been suggested to be a distinctive signature for structural phase transformations [54]. Interestingly, an abrupt decrease in the Poisson's ratio also occurs within the spin transition in magnesiosiderite, which displays an abnormal auxeticity with a negative Poisson's ratio of 0.6 at ~45.7 GPa. Compared to the extrapolated HS state magnesiosiderite, a maximum of approximately 240% reduction in the Poisson's ratio occurs within the spin transition. Previous studies have also reported a softening of the V_P/V_S ratio across the spin crossover in ferropericlase [8], but the recalculated Poisson's ratio from Ref. [8] remains positive within the spin transition. The phenomenon of a negative Poisson's ratio in magnesiosidertie suggests that significant auxetic behavior in minerals can be related to electronic spin transition-induced elastic anomalies.

Our results on the elasticity of magnesiosiderite across the spin transition can also provide mineral physics constraints on potential seismic detection of carbonate-rich regions in the Earth's lower mantle. A certain amount of carbon, on average of 3 wt. % CO_2, has been proposed to be transported deep into the Earth's interior, hosted in various forms, including CO_2-rich and hydrocarbon-rich fluids/melts, accessory minerals (carbonates, diamond, and graphite), and iron carbides [57-59]. Among those transported minerals, magnesite has been suggested to be the main host for carbons due to its ability to remain thermodynamically stable at relevant P-T conditions of the Earth's lower mantle [28-30]. Considering the average Fe/Mg molar ratio of ~0.12 in the Earth's mantle [60], the composition of carbonates in the mantle is likely to lie between magnesite and siderite, at a composition of $(Mg_{0.85}Fe_{0.15})CO_3$ [22, 36]. Assuming that the thermoelastic properties of ferromagnesite can be scaled linearly as a function of the iron concentration, our observed elastic anomalies in magnesiosiderite

[$(Mg_{0.35}Fe_{0.65})CO_3$] are expected to be reduced by a factor of approximately 4 for possible geophysical implications in the deep mantle. This suggests that a drastic softening of V_P (~10%) across the spin transition may occur in the subducted slab material enriched with ferromagnesite in the mid-lower mantle. Furthermore, the presence of carbonates such as magnetite and calcite in the deep Earth's interior has been used to explain low-velocity zones near the bottom of the Earth's lower mantle due to their relatively low compressional and shear velocities as compared with corresponding lower-mantle silicates [61]. Our study here further indicates that abnormal thermoelastic properties of iron-bearing magnesite across the spin transition in the mid lower mantle will have a significant influence on our understanding of seismic observations in the Earth's lower mantle.

Conclusion

We have experimentally measured the elasticity of the rhombohedral magnesiosiderite [$(Mg_{0.35}Fe_{0.65})CO_3$] across the electronic spin transition region at high pressures. Additionally, we have developed a thermoelastic model that corroborates our experimental findings for the elastic anomalies within the spin transition. Deciphering the electronic-induced elastic anomalies of crystals with lower symmetries both experimentally and theoretically in this study plays an important role in understanding its effects on the physical, chemical, and mechanical properties of materials, such as elasticity, acoustic velocity, and Poisson's ratio. The occurrence of elastic anomalies across electronic, structural, and magnetic transitions can be used to understand the interplay between the lattice, electronic and phonon band structures. Furthermore, the observed drastic softening of the compressional wave velocity and significant changes of V_P and V_S anisotropies across the spin transition are of great importance for constraining geophysical models of carbonates in the lower mantle.

Acknowledgements

J.F. Lin acknowledges supports from the US National Science Foundation (EAR-1053446 and EAR-1056670), the Sloan Foundation's Deep Carbon Observatory (DCO), and the Center for High Pressure Science and Technology Advanced Research (HPSTAR). The authors thank J.S. Kim for assistance in conducting 2-D Raman mapping and analysis of the sample at high pressures. The authors also thank R.H. Roberts for language polishing.

References:

[1] M. A. Carpenter, B. S. Li and R. C. Liebermann, Am Mineral **92**, 344 (2007).
[2] M. A. Carpenter, Am Mineral **92**, 328 (2007).
[3] M. A. Carpenter, Am Mineral **92**, 309 (2007).
[4] M. A. Carpenter, R. J. Hemley and H. K. Mao, J Geophys Res-Sol Ea **105**, 10807 (2000).
[5] R. Yang and Z. Q. Wu, Earth Planet Sc Lett **404**, 14 (2014).
[6] J. C. Crowhurst, J. M. Brown, A. F. Goncharov and S. D. Jacobsen, Science **319**, 451 (2008).
[7] H. Marquardt, S. Speziale, H. J. Reichmann, D. J. Frost and F. R. Schilling, Earth Planet Sc Lett **287**, 345 (2009).
[8] J. Yang, X. Y. Tong, J. F. Lin, T. Okuchi and N. Tomioka, Sci Rep-Uk **5** (2015).
[9] Z. Q. Wu, J. F. Justo and R. M. Wentzcovitch, Phys Rev Lett **110** (2013).
[10] J. F. Lin, J. J. Wu, J. Zhu, Z. Mao, A. H. Said, B. M. Leu, J. G. Cheng, Y. Uwatoko, C. Q. Jin and J. S. Zhou, Sci Rep-Uk **4** (2014).
[11] A. P. Kantor, S. D. Jacobsen, I. Y. Kantor, L. S. Dubrovinsky, C. A. McCammon, H. J. Reichmann and I. N. Goncharenko, Phys Rev Lett **93** (2004).
[12] I. Y. Kantor, C. McCammon and L. Dubrovinsky, J Alloy Compd **376**, 5 (2004).
[13] V. V. Struzhkin, H. K. Mao, J. Z. Hu, M. Schwoerer-Bohning, J. F. Shu, R. J. Hemley, W. Sturhahn, M. Y. Hu, E. E. Alp, P. Eng, et al., Phys Rev Lett **87** (2001).
[14] B. Chen, Z. Y. Li, D. Z. Zhang, J. C. Liu, M. Y. Hu, J. Y. Zhao, W. L. Bi, E. E. Alp, Y. M. Xiao, P. Chow, et al., P Natl Acad Sci USA **111**, 17755 (2014).
[15] B. Chen, L. L. Gao, B. Lavina, P. Dera, E. E. Alp, J. Y. Zhao and J. Li, Geophys Res Lett **39** (2012).
[16] D. C. Wallace, *Thermodynamics of crystals* (Courier Corporation, 1998).
[17] L. Landau, Nature **138**, 840 (1936).
[18] J. Liakos and G. Saunders, Philosophical Magazine A **46**, 217 (1982).
[19] J. F. Lin, S. Speziale, Z. Mao and H. Marquardt, Rev Geophys **51**, 244 (2013).
[20] Z. Mao, J. F. Lin, J. Liu and V. B. Prakapenka, Geophys Res Lett **38** (2011).
[21] J. F. Lin, H. Watson, G. Vanko, E. E. Alp, V. B. Prakapenka, P. Dera, V. V. Struzhkin, A. Kubo, J. Y. Zhao, C. McCammon, et al., Nat Geosci **1**, 688 (2008).
[22] J. F. Lin, J. Liu, C. Jacobs and V. B. Prakapenka, Am Mineral **97**, 583 (2012).
[23] J. Liu, J. F. Lin, Z. Mao and V. B. Prakapenka, Am Mineral **99**, 84 (2014).
[24] Q. Y. Hu, D. Y. Kim, W. G. Yang, L. X. Yang, Y. Meng, L. Zhang and H. K. Mao, Nature **534**, 241 (2016).
[25] Z. Q. Wu and R. M. Wentzcovitch, P Natl Acad Sci USA **111**, 10468 (2014).
[26] R. Dasgupta, M. M. Hirschmann and A. C. Withers, Earth Planet Sc Lett **227**, 73 (2004).

[27] R. Dasgupta and M. M. Hirschmann, Earth Planet Sc Lett **298**, 1 (2010).
[28] C. Biellmann, P. Gillet, F. Guyot, J. Peyronneau and B. Reynard, Earth Planet Sc Lett **118**, 31 (1993).
[29] M. Isshiki, T. Irifune, K. Hirose, S. Ono, Y. Ohishi, T. Watanuki, E. Nishibori, M. Takata and M. Sakata, Nature **427**, 60 (2004).
[30] A. R. Oganov, S. Ono, Y. Ma, C. W. Glass and A. Garcia, Earth Planet Sc Lett **273**, 38 (2008).
[31] V. Cerantola, C. McCammon, I. Kupenko, I. Kantor, C. Marini, M. Wilke, L. Ismailova, N. Solopova, A. Chumakov, S. Pascarelli, et al., Am Mineral **100**, 2670 (2015).
[32] A. Mattila, T. Pylkkanen, J. P. Rueff, S. Huotari, G. Vanko, M. Hanfland, M. Lehtinen and K. Hamalainen, J Phys-Condens Mat **19** (2007).
[33] B. Lavina, P. Dera, R. T. Downs, V. Prakapenka, M. Rivers, S. Sutton and M. Nicol, Geophys Res Lett **36** (2009).
[34] H. Shi, W. Luo, B. Johansson and R. Ahuja, Phys Rev B **78** (2008).
[35] H. Hsu and S.-C. Huang, Phys Rev B **94**, 060404 (2016).
[36] J. Liu, J. F. Lin and V. B. Prakapenka, Sci Rep-Uk **5** (2015).
[37] F. Gaillard, M. Malki, G. Iacono-Marziano, M. Pichavant and B. Scaillet, Science **322**, 1363 (2008).
[38] A. G. Every, Phys Rev B **22**, 1746 (1980).
[39] R. Hill, P Phys Soc Lond B **65**, 396 (1952).
[40] S. S. Lobanov, A. F. Goncharov and K. D. Litasov, Am Mineral **100**, 1059 (2015).
[41] M. Born and K. Huang, *Dynamical theory of crystal lattices* (Clarendon Press ;

Oxford University Press, Oxford

New York, 1988), Oxford classic texts in the physical sciences.
[42] F. Birch, J Geophys Res **83**, 1257 (1978).
[43] See Supplemental Material at [url] for details on the data collection, data analysis, and thermoelastic modelling across the spin transition, which includes Refs. [8,9,22,23,31,33,38-40,42,44-53].
[44] H. K. Mao, J. Xu and P. M. Bell, J Geophys Res-Solid **91**, 4673 (1986).
[45] A. Polian, D. Vo-Thanh and P. Richet, Europhys Lett **57**, 375 (2002).
[46] J. Ostwald, W. Pazold and O. Weis, Appl Phys **13**, 351 (1977).
[47] S. V. Sinogeikin and J. D. Bass, Phys Earth Planet In **120**, 43 (2000).
[48] N. Rividi, M. van Zuilen, P. Philippot, B. Menez, G. Godard and E. Poidatz, Astrobiology **10**, 293 (2010).
[49] T. Tsuchiya, R. M. Wentzcovitch, C. R. S. da Silva and S. de Gironcoli, Phys Rev Lett **96** (2006).
[50] R. M. Wentzcovitch, J. F. Justo, Z. Wu, C. R. S. da Silva, D. A. Yuen and D. Kohlstedt, P Natl Acad Sci USA **106**, 8447 (2009).
[51] M. J. P. Musgrave, *Crystal acoustics; introduction to the study of elastic waves and vibrations in crystals* (Holden-Day, San Francisco,, 1970), Holden-Day series in mathematical physics.
[52] C. Sanchez-Valle, S. Ghosh and A. D. Rosa, Geophys Res Lett **38** (2011).
[53] D. Mainprice, Comput Geosci **16**, 385 (1990).
[54] G. N. Greaves, A. L. Greer, R. S. Lakes and T. Rouxel, Nat Mater **10**, 823 (2011).
[55] R. E. A. McKnight, T. Moxon, A. Buckley, P. A. Taylor, T. W. Darling and M. A. Carpenter, J Phys-Condens Mat **20** (2008).
[56] D. Li, T. Jaglinski, D. S. Stone and R. S. Lakes, Appl Phys Lett **101** (2012).
[57] M. J. Walter, S. C. Kohn, D. Araujo, G. P. Bulanova, C. B. Smith, E. Gaillou, J. Wang, A. Steele and S. B. Shirey, Science **334**, 54 (2011).

[58] T. Stachel, G. P. Brey and J. W. Harris, Elements **1**, 73 (2005). [59] Y. N. Palyanov, Y. V. Bataleva, A. G. Sokol, Y. M. Borzdov, I. N. Kupriyanov, V. N. Reutsky and N. V. Sobolev, P Natl Acad Sci USA **110**, 20408 (2013).
[60] W. F. Mcdonough and S. S. Sun, Chem Geol **120**, 223 (1995).
[61] M. L. Marcondes, J. F. Justo and L. V. C. Assali, Phys Rev B **94**, 104112 (2016).